Biophysical *Journal*
Article

Fluid-gel coexistence in lipid membranes under differential stress

Samuel L. Foley,[1] Amirali Hossein,[1,2] and Markus Deserno[1,*]
[1]Department of Physics, Carnegie Mellon University, Pittsburgh, Pennsylvania and [2]Eunice Kennedy Shriver National Institute of Child Health and Human Development, Bethesda, Maryland

ABSTRACT A widely conserved property of many biological lipid bilayers is their asymmetry. In addition to having distinct compositions on its two sides, a membrane can also exhibit different tensions in its two leaflets, a state known as differential stress. Here, we examine how this stress can influence the phase behavior of the constituent lipid monolayers of a single-component membrane. For temperatures sufficiently close to, but still above, the main transition, molecular dynamics simulations show the emergence of finite gel domains within the compressed leaflet. We describe the thermodynamics of this phenomenon by adding two empirical single-leaflet free energies for the fluid-gel transition, each evaluated at its respective asymmetry-dependent lipid density. Finite size effects arising in simulation are included in the theory through a geometry-dependent interfacial term. Our model reproduces the phase coexistence observed in simulation. It could therefore be used to connect the "hidden variable" of differential stress to experimentally observable properties of the main phase transition. These ideas could be generalized to any first-order bilayer phase transition in the presence of asymmetry, including liquid-ordered/liquid-disordered phase separation.

SIGNIFICANCE Despite the ubiquity of asymmetric membranes, they have not been studied nearly to the same extent as their symmetric analogs. This was largely due to the difficulty of preparing asymmetric model membranes, a challenge only recently overcome. An important but still poorly understood feature is the stress state in asymmetric membranes, which couples to numerous properties. It was recently shown to give rise to a stiffening transition beyond sufficiently high asymmetry due to the emergence of gel domains in the compressed leaflet. In this work we introduce a theoretical model for this transition, which provides a way to infer the stress state of a membrane through observation of phase coexistence, and has general implications for phase behavior in asymmetric systems.

INTRODUCTION

Lipid bilayer asymmetry is a widely conserved biomembrane property across nearly all of Eukarya (1–4). As an example, it is well known that the composition of the plasma membrane of nucleated cells is asymmetric with respect to the exoplasmic and cytosolic leaflets (3). Such membrane states are not in thermodynamic equilibrium, but are quasistatic states maintained out-of-equilibrium by various active and passive biological processes (5). The existence of composition asymmetry in cellular membranes has been known since the 1970s (6), but interest in the study of asymmetric membranes and their role in the physical biology of cells has grown considerably in recent years, in part due to recent breakthroughs in experimental methods for preparing asymmetric model membranes (7–14). These simplified systems allow researchers to probe the fundamental consequences of membrane asymmetry without the added complexity of the myriad of proteins and cytoskeletal structures present in vivo.

However, composition difference is only one of the ways in which a membrane can be asymmetric; there is also the possibility of a difference in mechanical leaflet tension. Such a situation can arise if the lipid density differs between the two layers of the membrane, for instance, to balance curvature stresses resulting from mismatch of lipid spontaneous curvatures on the two sides. Differential stress could have important consequences for membrane-dependent processes in the cell, but the presence of stress asymmetry is currently something of a hidden variable, as it is very difficult to measure directly. This is not just a problem in living systems, but a difficulty which extends to the recently unlocked playground of asymmetric model membranes. It points to an important insight that is missing from these asymmetric

---

Submitted April 8, 2022, and accepted for publication July 12, 2022.

*Correspondence: deserno@andrew.cmu.edu

Editor: Michael Koslov.
https://doi.org/10.1016/j.bpj.2022.07.021

© 2022 Biophysical Society.

vesicle preparation protocols: a way to determine what differential stress, if any, will be present in a newly created vesicle. Without an understanding of the consequences of stress asymmetry and when it can be expected in idealized membranes, there is little hope for understanding its potential role in living cells.

It has been shown in simulation that beyond some critical threshold asymmetry, differential stresses can lead to a stiffening transition in compositionally symmetric bilayers (15), wherein the bending modulus increases significantly. More recent work has illustrated that the formation of highly ordered domains might play a role in this transition (16). This phenomenon could explain experimental results where asymmetric vesicles have membrane bending rigidities significantly larger than would be naïvely expected (17–19), since it is possible that model asymmetric membranes are inadvertently assembled with differentially stressed leaflets. At present, this possibility has not been experimentally investigated.

In an effort to help address this issue, and to gain a better general understanding of the thermodynamics of differentially stressed membranes, we develop in this work an idealized theory of the fluid-gel transition in single-component number-asymmetric bilayers and test it against simulations. We accomplish this by introducing an empirical monolayer free energy constructed from observable parameters, such as rest area per lipid a_ℓ and monolayer area compressibility modulus $K_{A,\mathrm{m}}$. By combining two such free energies evaluated at the appropriate specific area in each of the two leaflets, we arrive at a composite free energy that can be used to numerically deduce monolayer phase coexistence diagrams. In a way, the density difference between the leaflets "detunes" their transition temperature, which due to their elastic coupling broadens the phase transition—a very generic phenomenon that has been previously investigated by Markin and Kozlov using slightly different methods (20).

The important experimental signal our theory predicts is a fluid-gel coexistence region just above the main transition temperature T_{gel}, which indeed matches the observation from simulation. The size of the coexistence region, and accordingly the coexistence onset temperature, increases with increasing asymmetry. The differential stress in our system arises through a mismatch in the number of lipids in each individual monolayer, quantified by an asymmetry parameter

$$\delta n = \frac{N_+ - N_-}{N_+ + N_-}, \tag{1}$$

where N_+ and N_- are the number of lipids in the overfilled and underfilled leaflets, respectively.

An interesting insight gleaned from our approach is that this behavior is in no way unique to lipid bilayers; similar coexistence phenomena should occur in any analogous asymmetric composite system. This includes one of the earliest and simplest thermodynamic fluid models ever studied, the van der Waals gas. We utilize this connection to introduce our theoretical idea in a setting that is familiar and where the free energy is well known, before we translate it to the bilayer case, for which we need to make some empirical assumptions concerning the leaflet free energy. In addition to numerical results, approximate analytical expressions for the fluid/gel phase coexistence are obtained from the proposed theory, the simplest of which states that the temperature increment above the main transition for which coexistence sets in varies linearly with asymmetry. To lowest order, the slope of the coexistence onset boundary is found to depend on the monolayer specific latent heat and specific area difference of the main transition, the fluid area compressibility modulus, and the main transition temperature T_{gel}.

At the small system sizes typical of molecular dynamics (MD) simulations, finite size effects ordinarily neglected at the level of macroscopic thermodynamics become significant. To appropriately compare the results from simulation to the theory, we introduce nonextensive geometry-dependent free energy terms to account for the unfavorable fluid-gel domain interface that arises in the coexistence region.

METHODS

Theory

Analogous van der Waals system

Consider a system consisting of two cylinders filled with N_+ and $N_- \leq N_+$ particles of a van der Waals gas, as illustrated in Fig. 1 *a*, with critical temperature T_c and critical specific volume v_c. The two cylinders are capped with freely moving pistons that are connected such that the two subsystems are constrained to occupy identical volumes V. The system is exposed to constant external pressure p. We now wish to explore what occurs in the compressed subsystem in the vicinity of the phase transition temperature.

Let us write the Helmholtz free energy per molecule for one of these cylinders in units of $k_\mathrm{B}T_\mathrm{c}$ (21):

$$f_1(T, v_\pm) = -T\left[1 + \log\frac{\left(v_\pm - \frac{1}{3}\right)T^{3/2}}{c}\right] - \frac{9}{8v_\pm}. \tag{2}$$

In this expression T and $v_\pm$ are the temperature and specific volume in the $+/-$ cylinder, measured in units of T_c and v_c, respectively. The constant c is irrelevant for our purposes and for simplicity we set it to 1. With this we can write down the total free energy for the composite system,

$$F(T, V, N_+, N_-) = N_+ f_1\left(T, \frac{V}{N_+}\right) + N_- f_1\left(T, \frac{V}{N_-}\right). \tag{3}$$

One should be careful to note that V in this expression is the volume of one cylinder, not the total volume of the system, and so the work corresponding

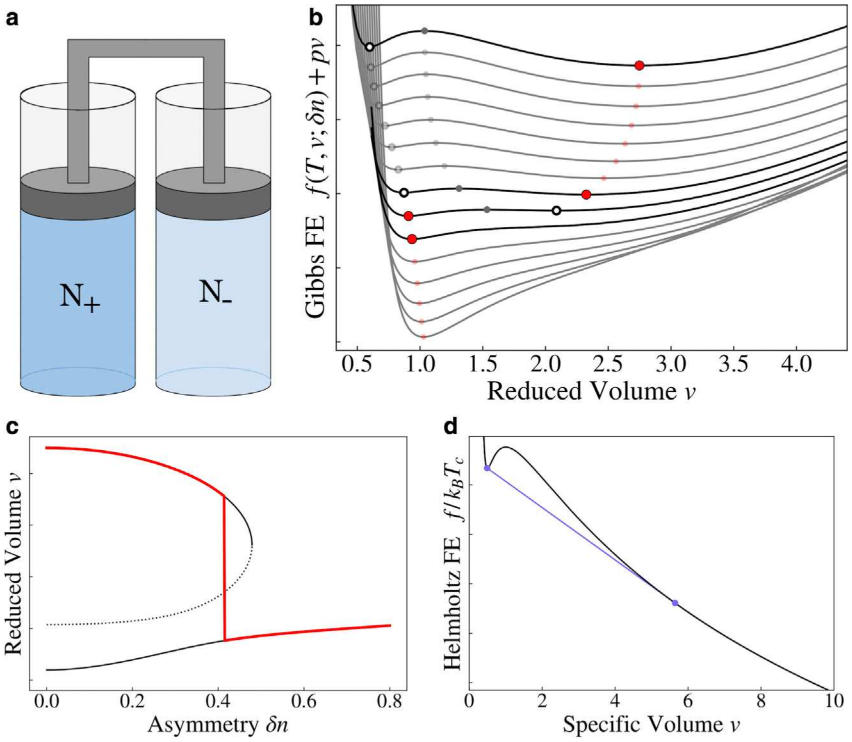

FIGURE 1 (*a*) Schematic representation of the coupled van der Waals system. (*b*) Plots of $f(T, v; \delta n) + pv$ as a function of v for $p_{\mathrm{ext}} = 0.22$, $T = 0.891$ for the asymmetric van der Waals system. Each curve corresponds to one of 15 values of δn between 0 and 0.8. Red points are the global minimum of each curve, with open black circles for local minimum. The local maximum is indicated by a small gray point. For clarity, the curves have been shifted downward for successive values of δn. (*c*) Plot of minima (*solid curves*) and maximum (*dotted*) for the free energies in part (*b*) as a function of asymmetry δn. The bold red curve tracks the global minimum, i.e., the equilibrium value of v, corresponding to the red points above. (*d*) Helmholtz free energy per particle of a van der Waals fluid emphasizing the nonconvex "bump" region (*black curve*). Double-tangent construction shown in blue. To see this figure in color, go online.

to a change dV at constant temperature is not $-p\mathrm{d}V$, but $-2p\mathrm{d}V$, hence $(\partial F/\partial V)_T = -2p$. If we define $N_0 = \frac{1}{2}(N_+ + N_-)$ and $\delta n = (N_+ - N_-)/2N_0$, and let $v = V/N_0$, then the free energy per particle of the entire system, $f(T, v) = F/2N_0$, can be written as

$$f(T,v;\delta n) = \frac{1}{2}\left[(1+\delta n)f_1\left(T,\frac{v}{1+\delta n}\right) + (1-\delta n)f_1\left(T,\frac{v}{1-\delta n}\right)\right]. \tag{4}$$

The parameter δn determines the extent of number asymmetry; it is the percentage difference between $N_\pm$ and N_0. For brevity, we often omit the explicit δn dependence when writing $f(T, v)$. In this formulation, we have restored the expected relation $(\partial f/\partial v)_T = -p$. This variable v as defined above has units of specific volume; however, it is important to note that it is not the volume per particle of either compartment. Its relation to the actual specific volumes of the subsystems, $v_\pm$, is

$$v^{-1} = \frac{1}{2}\left(v_+^{-1} + v_-^{-1}\right). \tag{5}$$

This is the harmonic mean of the specific volumes in each subsystem, or equivalently the specific volume corresponding to the average density. We simply call it the *reduced volume* of the system.

In equilibrium under external pressure p, the system will take on the volume which minimizes the Gibbs free energy, $g(T,p) = \min_v g(T,p;v) = \min_v\{f(T,v) + pv\}$. Fig. 1 *b* shows examples of $g(T,p;v)$ curves over a range of values of the asymmetry parameter δn for a system at temperature $T = 0.891$ and subject to external pressure $p_{\mathrm{ext}} = 0.22$. An ordinary system (one cylinder, no asymmetry) of this gas is in the vapor phase at this temperature and pressure, as the phase transition temperature is $T_{\mathrm{lv}} \approx 0.88$. Examining the uppermost curve in Fig. 1 *b*, for which $\delta n = 0$, the large-volume minimum, corresponding to the vapor phase, is the global minimum. This is as expected, because when $\delta n = 0$, the composite system is simply two identical cylinders of van der Waals gas under identical conditions. However, at non-zero values of δn, the low-volume minimum eventually becomes the global minimum, indicating that a first-order phase transition occurs as asymmetry is increased. At sufficiently high asymmetry, the large-volume minimum disappears entirely.

Rather than plotting individual $g(T,p;v)$ curves for discrete values of δn, we can plot only the locations of the minima as a function of δn. This is shown in Fig. 1 *c* for the same state point as the first plot, and clearly illustrates a transition point, as well as the end of the metastable large-volume minimum, which "annihilates" with the location of the unstable maximum.

However, our analysis up to this point has been overly simple, in that it neglects the Maxwell construction and its implications for phase coexistence. The Maxwell construction arises from the fact that the system can achieve an overall lower free energy in the nonconvex "bump" region by splitting into two domains with specific volumes corresponding to the end points of the double-tangent line, which makes the free energy overall convex. In this way, the true thermodynamic free energy is the convex envelope of the curve in Fig. 1 *d*, shown in blue. (Note: the free energy curve in Fig. 1 *d* is for a lower temperature than our previous example because the free energy curve has a more exaggerated shape, making it easier to see the tangent line.) The double-tangent construction then also determines what fraction ϕ of molecules is currently in the liquid or vapor state in an individual subsystem through the well-known lever rule:

$$\phi_{\mathrm{vap},\pm} = \frac{v_\pm - v_{\mathrm{L}}}{v_{\mathrm{R}} - v_{\mathrm{L}}} \quad \text{and} \quad \phi_{\mathrm{liq},\pm} = 1 - \phi_{\mathrm{vap},\pm}, \tag{6}$$

where v_{L} and v_{R} are the left and right end points of the double tangent.

Finally, by minimizing the correct total free energy constructed from the convex single-subsystem free energies, we can map out the phase behavior of the compressed container over a range of T and δn. Fig. 2 displays the fraction of liquid in the compressed van der Waals subsystem as a function of temperature and asymmetry. For $\delta n > 0$, upon cooling the system, the sharp first-order vapor-liquid phase transition is preceded by an extended region of liquid-vapor coexistence in the compressed subsystem. The temperature at which this behavior begins can be significantly larger than the

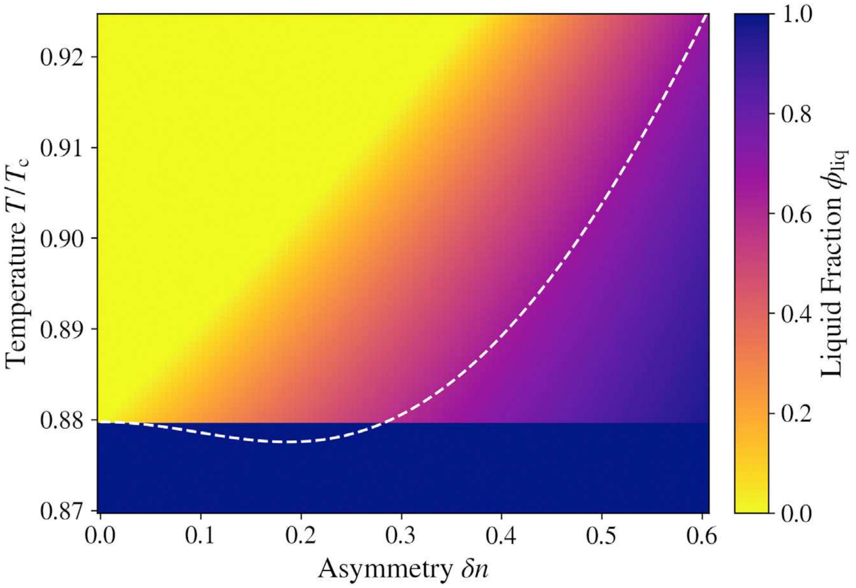

FIGURE 2 Condensed liquid fraction of compressed (+) van der Waals subsystem as a function of temperature T and asymmetry δn. Yellow corresponds to 100% vapor, dark blue to 0% vapor (100% liquid), and color gradient to intermediate values (liquid-vapor coexistence). The calculations were done for $p = 0.22$. White dashed curve: sharp transition predicted in absence of double-tangent construction. To see this figure in color, go online.

ordinary transition temperature $T_{\rm lv}$, and increases approximately linearly with increasing asymmetry.

Lipid membrane free energy

Our van der Waals explorations above served as a primer for our true goal: we now follow the same steps, but for a lipid bilayer system rather than coupled containers of van der Waals fluid. Each cylinder is replaced by a single-component lipid monolayer of the same species. The condition of equal volumes coupled to an external pressure is replaced by the two monolayers being constrained to occupy the same frame area A under conditions of zero net bilayer tension, that is, $(\partial F/\partial A)_T = \Sigma = \Sigma_+ + \Sigma_- = 0$. Almost all previous arguments and techniques carry over to the membrane case, with the spatial dimension reduced from 3 to 2. We additionally need to augment the theory thus developed to account for finite-size effects encountered in simulation. Before that, one immediate complication is that the free energy for a lipid monolayer is not as easy to write down as for a van der Waals fluid.

Detailed investigations into the statistical mechanics of the membrane main phase transition and lipid monolayer equation of state have been carried out in the past; for perspectives on this, see the reviews by, e.g., Nagle (22) or Marsh (23). For our purposes, we need not delve into these details. Instead, we construct here a simple phenomenological free energy for a single monolayer as a function of area. We start with the area compressibility moduli of the fluid and gel phases, $K_{A,\rm m,fl}$ and $K_{A,\rm m,gel}$, which are readily measurable in both simulation and experiment. These two constants determine the curvature of the free energy minima corresponding to the fluid and gel states, as the free energy can be Taylor expanded to second order about the rest area A_0 of either the fluid or gel phase in the form

$$F_{\rm m}(A) = \frac{1}{2}K_{A,\rm m}\frac{(A - A_0)^2}{A_0} . \tag{7}$$

This can be recast as free energy per molecule as a function of area per lipid $a = A/N$,

$$f_{\rm m}(a) = \frac{F_{\rm m}(Na)}{N} = \frac{1}{2}k_{A,\rm m}(a - a_\ell)^2 , \tag{8}$$

in which $a_\ell = A_0/N$ and $k_{A,\rm m} = K_{A,\rm m}/a_\ell$. Taking this expression as the local form of the free energy in the vicinity of each phase's preferred area, we can construct a full free energy by interpolating between these two with a barrier. For the moment, let us assume that we are at the coexistence temperature, where the two phases have the same free energy. We then write

$$\bar{f}_{\rm m}(a) = \begin{cases} \frac{1}{2}k_{A,\rm m,gel}\left(a - a_{\ell,\rm gel}\right)^2 & a \le a_{\ell,\rm gel} \\ b \bullet {\rm B}(a) & a_{\ell,\rm gel} < a < a_{\ell,\rm fl} \\ \frac{1}{2}k_{A,\rm m,fl}\left(a - a_{\ell,\rm fl}\right)^2 & a \ge a_{\ell,\rm fl} \end{cases} , \tag{9}$$

where the barrier function ${\rm B}(a)$ is given by

$$\begin{aligned} {\rm B}(a) = {} & \left[\left(k_{A,\rm m,fl} - k_{A,\rm m,gel}\right)a - k_{A,\rm m,fl}a_{\ell,\rm gel} + k_{A,\rm m,gel}a_{\ell,\rm fl}\right] \\ & \times \frac{\left(a - a_{\ell,\rm fl}\right)^2\left(a - a_{\ell,\rm gel}\right)^2}{2\left(a_{\ell,\rm fl} - a_{\ell,\rm gel}\right)^3} . \end{aligned} \tag{10}$$

This function ${\rm B}(a)$ is simply the unique degree 5 polynomial such that $\bar{f}_{\rm m}(a)$ is twice differentiable at $a_{\ell,\rm fl}$ and $a_{\ell,\rm gel}$, when the parameter b is equal to 1. The precise functional form of this barrier function far from the minima is not of immediate practical importance for our purpose, as nonconvex portions of the free energy are replaced by the convex envelope in the thermodynamic limit. However, in the case of systems of finite size, which we treat in the next section, it is sometimes useful to allow this barrier to be adjusted. This is the purpose of the parameter b, which simply scales the height of the barrier, thereby also adjusting its steepness. For the moment, it can be assumed to be 1. The function $\bar{f}_{\rm m}(a)$ is shown as the black curve in Fig. 3.

We can tune the free energy difference between the two minima by adding a linear term with slope $-\sigma$,

$$f_{\rm m}(a,\sigma) = \bar{f}_{\rm m}(a) - \sigma a . \tag{11}$$

This will contribute a term $-\sigma$ to the monolayer tension $\Sigma_{\rm m} = \partial f_{\rm m}/\partial a$. However, we can also reinterpret it as a stand-in for temperature

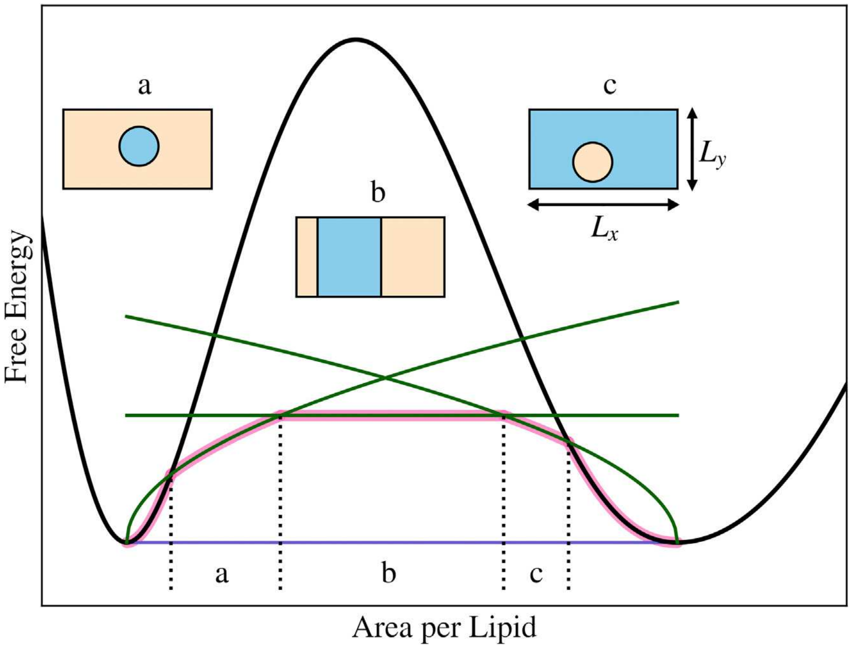

FIGURE 3 Schematic plot of $f_{\mathrm{m}}(a,0) = \bar{f}_{\mathrm{m}}(a)$ along with finite-size corrections from Eqs. 14 and 15. The homogeneous free energy is shown as the solid black curve, with double tangent in blue. Free energy contributions due to interfacial terms ΔF_γ shown in green. The resulting monolayer free energy $F_{\mathrm{m}}(a,\sigma,N)$, determined according to Eq. 16, is indicated by the highlighted pink path in the double-tangent region. Schematic illustrations of lipid phase coexistence geometries are shown and labeled according to the corresponding interval of the free energy (bottom). To see this figure in color, go online.

dependence in the following way: close to the liquid-gel phase boundary (pb), the Clausius-Clapeyron relation

$$\left(\frac{\mathrm{d}\Sigma_{\mathrm{m}}}{\mathrm{d}T}\right)_{\mathrm{pb}} = -\frac{\Delta q_{\mathrm{m}}}{T\Delta a}\,, \tag{12}$$

which gives the slope of the coexistence line in the tension-temperature plane, allows us to effectively approximate small changes in temperature via equivalent changes in leaflet tension, given the monolayer specific latent heat Δq_{m} and specific area change Δa of the fluid-gel transition. In this way, despite not knowing the exact temperature dependence of the monolayer free energy, we can construct a meaningful linear-order approximation to the temperature dependence using the conversion

$$\sigma \approx \frac{\Delta q_{\mathrm{m}}}{T_{\mathrm{gel}}\Delta a}\left(T - T_{\mathrm{gel}}\right)\,. \tag{13}$$

We are now prepared to construct fluid-gel phase coexistence diagrams for differentially stressed bilayers in the thermodynamic limit, akin to Fig. 2. Before we can compare our results to simulation, however, we have one more obstacle to surmount.

Finite-size corrections

The double-tangent construction only truly represents the shape of the free energy of coexistence in the thermodynamic limit $N \to \infty$, where only $\mathcal{O}(N)$ terms remain. Nonextensive quantities, such as terms arising due to interactions at interfaces, become negligible in comparison to the bulk in this limit. Taking into account finite-size effects requires including an $\mathcal{O}(N^{(d-1)/d})$ free energy contribution, in our case arising from the contact line(s) between coexisting fluid and gel phases.

Consider a single monolayer of area A containing N lipids, with N_{gel} lipids in the gel phase coexisting with $N_{\mathrm{fl}} = N - N_{\mathrm{gel}} > N_{\mathrm{gel}}$ lipids in the fluid phase. If these gel lipids have coalesced in the form of a circular domain with line tension γ and radius R, then the free energy contribution due to the interface between the phases is

$$\Delta F_\gamma = 2\pi R\gamma = 2\gamma\sqrt{\pi N_{\mathrm{gel}} a_{\mathrm{L}}}\,, \tag{14}$$

with N_{gel} being determined by the lever rule as before. One can also imagine the reverse situation, where there exists a domain of fluid within an otherwise gel leaflet; the only changes to the above expression are the replacement of N_{gel} with N_{fl} and a_{L} with a_{R}.

Under periodic boundary conditions, it is possible for a gel domain in a leaflet to connect to itself across one of the periodic directions of the simulation box, creating a band of gel, as shown in Fig. 3 *b*. The nonextensive free energy penalty is then simply

$$\Delta F_\gamma = 2\gamma L\,, \tag{15}$$

where L is the box length along the direction of the band (L_y in Fig. 3), independent of the size of the domain.

Whether or not a system will undergo phase separation and coexistence at a given area ultimately depends on whether the double-tangent free energy plus interface term is lower than the homogeneous free energy (no Maxwell construction). The equilibrium free energy for an individual monolayer in the double-tangent region is therefore

$$F_{\mathrm{m}}(a,\sigma,N) = \min\left\{\begin{array}{c} Nf_{\mathrm{m}}(a,\sigma) \\ Nf^*_{\mathrm{m}}(a,\sigma) + \Delta F_\gamma \end{array}\right\}, \tag{16}$$

where $f^*_{\mathrm{m}}(a,\sigma)$ is the convex envelope of $f_{\mathrm{m}}(a,\sigma)$. It is important to bear in mind that the minimization in Eq. 16 must be carried out over all possible forms of ΔF_γ. Note also that, as the interfacial tension γ increases, the monolayer becomes more likely to continue along the nonconvex homogeneous free energy, as can be seen clearly in Fig. 3.

In close analogy to Eq. 4, the total free energy for a composite asymmetric system of finite size is then

$$\begin{aligned} F(a,\sigma,N_0;\delta n) = {} & F_{\mathrm{m}}\left(\frac{a}{1+\delta n},\sigma,N_0(1+\delta n)\right) \\ & + F_{\mathrm{m}}\left(\frac{a}{1-\delta n},\sigma,N_0(1-\delta n)\right). \end{aligned} \tag{17}$$

This is the free energy that must be used when calculating the gel fraction of an individual membrane leaflet to obtain agreement with MD simulations, which are often thermodynamically very small systems.

For completeness, we wish to point out that there is an additional complication that arises in the case of a circular domain. The two-dimensional version of the Young-Laplace equation, $\Sigma_{\mathrm{m,in}} - \Sigma_{\mathrm{m,ext}} = \gamma / R$, tells us that the tension is different in the two phases when the interface is curved. This means that the area per lipid for these two phases is not required to reside exactly on the endpoints of the double-tangent construction, which by definition corresponds to states of equal tension, and is assumed in the lever rule. For this situation, the equilibrium state is found by minimizing the free energy while allowing the two phase areas to vary, subject to the constraints given by the Young-Laplace equation and that the sum of the two domain areas gives the total area. This complication is considered in more detail in the work by Tröster et al. (24). Fortuitously, this problem is not of imminent concern in this work. In our Martini model simulations, the zero-curvature band state is the only observed domain topology. For the Cooke model, we find that the fluid-gel line tension γ is negligible, in the sense that among the three contributions to a domain's free energy—chemical potential difference between the phases, stress reduction, and line tension—the balance happens between the first two. This is unusual from the point of view of classical nucleation theory, where a bulk term competes against an interface term, and it arises since nucleation is driven by bulk stress and opposed by the creation of an unfavorable bulk phase.

An analytical result

Before charging ahead to numerical results based on simulation data, let us take a moment to glean some analytical insights from the framework now established. Its most important feature is the appearance of phase coexistence at a temperature T_{pc} slightly above the main phase transition, as we have seen previously in the compressed van der Waals subsystem. For an asymmetric membrane, this is the transition to a state where finite gel domains appear in the otherwise fluid-compressed leaflet. Given δn, what is the temperature $T_{\mathrm{pc}} > T_{\mathrm{gel}}$ at which this occurs?

In the thermodynamic limit, this corresponds to finding the combination of δn and T (or rather, σ, in our case) that results in a_+ being equal to the right endpoint area of the double tangent, a_{R}. Our first task then is to derive a simple approximation for a_{R} in terms of the known quantities used to construct our free energy. Taking the two minima as parabolic and using the definition of the double tangent, one can show that the area difference $\delta a = a_{\ell,\mathrm{fl}} - a_{\mathrm{R}}$ is approximately

$$\delta a \approx \frac{1}{k_{A,\mathrm{m,fl}}} \frac{\Delta f_0}{\Delta a_0}\ , \tag{18}$$

where $\Delta a_0 = a_{\ell,\mathrm{fl}} - a_{\ell,\mathrm{gel}}$ and $\Delta f_0 = f_{\mathrm{m}}(a_{\ell,\mathrm{gel}}) - f_{\mathrm{m}}(a_{\ell,\mathrm{fl}})$ are the area and free energy differences between the two minima. Fig. 4 shows a schematic of the quantities involved. $\Delta f_0 = \sigma \Delta a_0$ by construction in Eq. 11, and so we arrive at the simple expression $\delta a \approx \sigma / k_{A,\mathrm{m,fl}}$. (Intuitively, a change of σ changes the minimum by $\sigma / k_{A,\mathrm{m,fl}}$ but leaves the contact point of the double tangent [approximately] unchanged.)

To reach our goal, we now must find an approximation for a_+ in terms of δn, and then replace δa on the left-hand side of Eq. 18 with $a_{\ell,\mathrm{fl}} - a_+(\delta n)$. The condition of zero bilayer tension $\Sigma = \partial F / \partial A = 0$ can be used to solve for the equilibrium area of the bilayer as a function of asymmetry, $A(\delta n)$, which in the Hookean approximation can be shown to be $A(\delta n) = A_0(1 - \delta n^2)$, where $A_0 = N_0 a_{\ell,\mathrm{fl}}$ is the rest area of the bilayer at zero asymmetry (25). Substituting this into the relation $a_+ = a/(1 + \delta n)$ brings us to $a_+ = a_{\ell,\mathrm{fl}}(1 - \delta n)$, and combining it with our previous result, the approximate equation for the coexistence-onset boundary is the remarkably simple expression

$$a_{\ell,\mathrm{fl}} \delta n \approx \frac{\sigma}{k_{A,\mathrm{m,fl}}}\ . \tag{19}$$

We can re-express this in terms of temperature using Eq. 13 to produce our final result,

$$\delta n \approx \frac{\Delta q_{\mathrm{m}}}{K_{A,\mathrm{m,fl}} \Delta a} \left(\frac{T_{\mathrm{pc}}}{T_{\mathrm{gel}}} - 1 \right), \tag{20a}$$

or equivalently,

$$T_{\mathrm{pc}} \approx T_{\mathrm{gel}} \left(1 + \frac{K_{A,\mathrm{m,fl}} \Delta a}{\Delta q_{\mathrm{m}}} \delta n \right). \tag{20b}$$

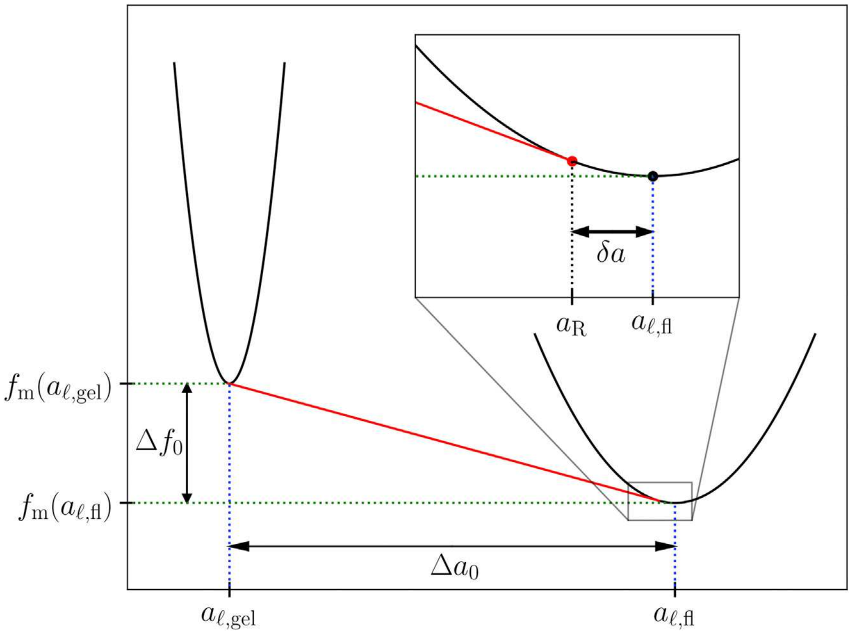

FIGURE 4 Illustration of the quantities involved in deriving the coexistence-onset boundary approximation. To see this figure in color, go online.

In which we have made use of $K_{A,\mathrm{m,fl}} = a_{\ell,\mathrm{fl}} k_{A,\mathrm{m,fl}}$. The prediction in Eq. 19 was used to generate the dashed lines in Fig. 5, further distinguishing the finite-size results from the thermodynamic limit and displaying that the slope of the phase boundary remains nearly the same for finite systems.

Within the same approximate regime, it can also be shown that the differential stress $\Delta\Sigma = \Sigma_{>} - \Sigma_{<} = 2K_{A,\mathrm{m,fl}}\delta n$. By substituting this into our previous result, we find the phase coexistence temperature as a function of the differential stress:

$$T_{\mathrm{pc}} \approx T_{\mathrm{gel}}\left(1 + \frac{\Delta\Sigma\Delta a}{2\Delta q_{\mathrm{m}}}\right). \tag{21}$$

Let us look at a specific case to get a sense for how big this effect is, taking DPPC and its transition from the fluid into the ripple phase at 41°C as an example. The change in area per lipid has been measured as $\Delta a = 0.15\mathrm{nm}^2$ (26) and the specific latent heat as $\Delta q = 8.1\ \mathrm{kcal/mol}$ (27). Taking $K_{A,\mathrm{m,fl}} = 120\ \mathrm{mN/m}$ (half a typical bilayer value (28)) and assuming (somewhat more daringly) that $\Delta q_{\mathrm{m}} = \Delta q$, we find that the onset of phase coexistence lies above the main phase transition by an amount

$$T_{\mathrm{pc}} - T_{\mathrm{gel}} \approx 1\ \mathrm{K} \times \frac{\delta n}{1\%} \approx 0.44\ \mathrm{K} \times \frac{\Delta\Sigma}{\mathrm{mN/m}}. \tag{22}$$

Each percentage point in asymmetry δn raises the temperature difference by about 1 degree; or alternatively, each additional mN/m in differential stress raises it by a little less than half a degree. Since (15) argues that spontaneous curvature differences across leaflets can give rise to differential stresses of several mN/m, temperature differences in the few degree range appear quite achievable.

Simulations

To evaluate the validity of the theory developed in the previous section, we performed MD simulations of asymmetric lipid bilayers using two coarse-grained (CG) lipid models: Martini (29) and a "flip-fixed" version of the Cooke model, modified to allow the simulation of differentially stressed membranes (25). Both models were run in anisotropic cuboid boxes such that $L_x > L_y$, with L_z being the box height in the bilayer normal direction. Fluctuations in area were only allowed to occur along the x-direction of the box, with L_y being held fixed. This anisotropic setup coaxes any gel domain large enough to connect via periodic boundary conditions to first do so along the shorter but inert y-direction. The resulting gel-band can easily change its size by changing its width, and it does not interfere with tension and area control along L_x (30).

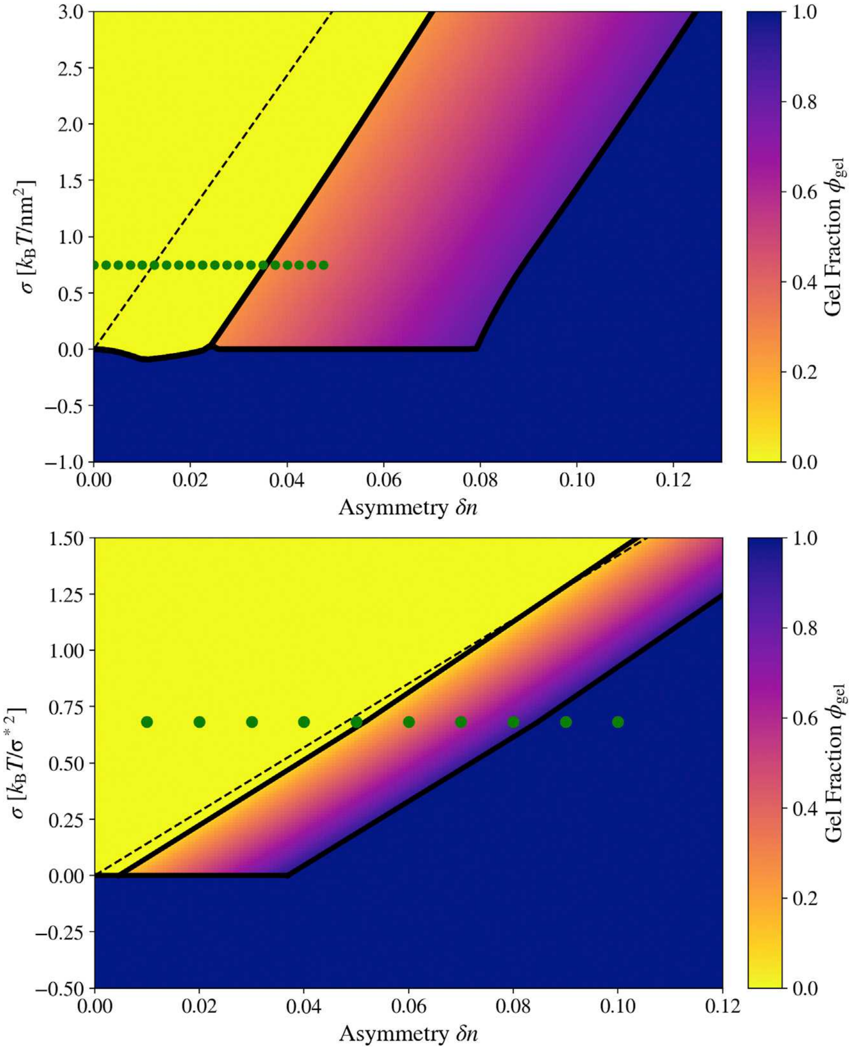

FIGURE 5 Gel fraction of compressed (+) leaflet of an asymmetric bilayer. Yellow corresponds to 0% gel (100% fluid), dark blue to 100% gel, with intermediate values given by color gradient (fluid-gel coexistence). Thick dark lines indicate the locations of discontinuous changes in gel fraction (and area). The thin dashed line indicates the coexistence-onset boundary in the thermodynamic limit as predicted by the approximation in Eq. 19. The parameters used to generate these diagrams come from fitting to membrane area data from simulations of 800 lipids. Top: Martini DLPC lipids at 297.5 K. Bottom: asymmetric Cooke lipids at $k_{\mathrm{B}}T = 1.36\epsilon$. Simulation state points are indicated by the green dots (data in Fig. 6). To see this figure in color, go online.

From these simulation trajectories we extracted the (projected) area per lipid, as well as gel and fluid fractions of the individual monolayers. Gel phase lipids were identified using a hidden Markov model (HMM) in a similar spirit to previous work by Sodt and co-workers (31,32). HMM methods were also used to separate trajectory snapshots belonging to different metastable states between which the systems alternated. For all quantities measured from sampled simulation data, after initial transient behaviors have decayed away, we calculated the error of the mean using a block averaging procedure (33) to correct for time correlation in the equilibrium time series.

Given that the two leaflets generally contain an unequal number of lipids, one might expect the resulting bending torques to curve the membrane and lead to buckled shapes. However, this cannot happen under periodic boundary conditions—at least not for small deviations from the flat state. The reason is that the area difference is proportional to the integral of the mean curvature, which in Monge gauge is a total divergence. Via Gauss' theorem, this integral can be shifted to the boundary, where the two contributions from opposite sides subsequently cancel. Hence, to lowest order shape changes cannot relax bending torques.

Martini simulations

CG Martini simulations were carried out using the martini_2.1 force field in GROMACS 5.1 (34) for systems containing a total of 800 DLPC lipids at a temperature of $T = 297.5$ K and a pressure of 1 bar, with $L_y = 8$ nm. For $\delta n = 0$, $\langle L_x \rangle = 28.41$ nm. We used a time step of $\delta t = 20$ fs and a 1.4 nm Verlet cutoff neighbor list updated every 10 steps. The relative dielectric constant was set to $\varepsilon_r = 15$. Temperature control was achieved using a Berendsen thermostat (35) with a time constant $\tau_T = 1$ ps, with pressure controlled along the fluctuating coordinate directions using a Berendsen barostat (35) with time constant $\tau_P = 3$ ps and isothermal compressibility $\kappa_T = 3 \times 10^{-5}$ Pa. Simulations were run for 20 values of the asymmetry parameter δn evenly spaced between 0 and 4.75%. These systems were equilibrated for 80 ns followed by 1.6 μs production runs.

Cooke simulations

Similar simulations were carried out using the flip-fixed Cooke CG lipid model (25,36). Simulations containing 800 (generic) lipids were carried out at a temperature of $k_B T = 1.36\,\varepsilon$ using a Langevin thermostat with friction constant of $\Gamma = 1.0\,\tau^{-1}$, and conditions of zero bilayer tension controlled by a modified Andersen barostat (37). The time step was set to $\delta t = 0.005\,\tau$, and L_y was fixed at 16 σ^* (σ^* being the CG length unit, not to be confused with tension). The $\delta n = 0$ simulation resulted in $\langle L_x \rangle = 28.50\,\sigma^*$. Individual runs were of duration $10^5\,\tau$, with the first $2 \times 10^4\,\tau$ being excluded from analysis as equilibration. Simulations were run for 10 values of asymmetry spaced evenly from 1 to 10%. All Cooke model simulations were run using the ESPResSo MD package (38).

HMMs

To compare the theoretical gel fraction values to those in simulation, we used a Gaussian HMM to classify each lipid into one of two states at each trajectory output step, interpreted as being either in the gel or in the fluid phase. This is an unsupervised learning process that is trained on chosen features that contain relevant information for each lipid at each step of a Markov process. All HMM calculations were carried out using the python package hmmlearn (39), which implements the Baum-Welch algorithm (40) for learning the model parameters and the Viterbi algorithm (41) for estimating the most likely hidden states along a trajectory.

For both Martini and Cooke, the primary feature of interest for a given lipid is the (magnitude of the) local hexatic order parameter, $|\psi_6|$, defined by

$$|\psi_6| = \left| \frac{1}{N} \sum_{k=1}^{N} e^{6i\theta_k} \right|, \tag{23}$$

where N is the number of neighbors and θ_k is the angle to neighbor k from a fixed axis. $|\psi_6|$ takes on values between 0 and 1, with 1 corresponding to a perfectly ordered hexatic crystal. For Martini, this order parameter is defined on a per-lipid-tail basis, whereas for Cooke (which lacks the distinction of separate tails) it is per-lipid. For the Cooke model, we found it necessary to include more training features to successfully infer lipid phases. These included the area per individual lipid, as determined by the lipid's Voronoi cell, as well as the distance to its nearest neighbor. Calculation of Voronoi diagrams and kd trees for efficient nearest-neighbor lookup were carried out using built-in functions provided by SciPy (42). Each HMM (one for each CG model) was trained on a simulation state point where fluid-gel coexistence had been visually observed, and then this trained model was used to infer lipid states in all other simulations for that model. An example of state labeling of a snapshot from a Cooke simulation is shown in Fig. S1.

When metastable state-switching was observed in Cooke simulations, we implemented an HMM trained on instantaneous area to classify individual trajectory steps into three states, interpreted as high area, low area, and transitional (see Fig. S2). For the Martini simulations, the HMM was trained on the overall fraction of gel in the compressed leaflet of the membrane in each snapshot. In Fig. 6, simulations with metastable state switching have two data points, with the black (stable) data point being the one in best agreement with the theory. Only the black data points were used in the fits shown.

Fitting to theory

Of the parameters appearing in the finite-size free energy, $K_{A,\mathrm{m,fl}}$, $K_{A,\mathrm{m,gel}}$, $a_{\ell,\mathrm{fl}}$, and $a_{\ell,\mathrm{gel}}$ are fairly easily measured in symmetric membrane simulations at temperatures above and below the gel transition as appropriate, and extrapolated to obtain approximate values at a given state of interest. The remaining quantities b, σ, and γ are trickier, and so are determined by fitting to data from a series of asymmetric simulations. In principle, if the monolayer specific latent heat Δq_m and gel transition temperature T_{gel} are known with precision, σ can be approximated from Eq. 13, and need not be a fitting parameter. However, in what follows we infer σ from the fit, allowing the fitting process to find the effective tension value corresponding the to the simulation temperature.

There is some choice available in what data are used for fitting. Two important quantities we measured in simulation for which we can also make predictions with this theory are the membrane area (or reduced area a) as a function of δn, as well as the gel fraction of an individual leaflet as described above. Calculating these amounts to finding (numerically) the area which minimizes the free energy for the system and applying the lever rule for each individual monolayer.

RESULTS

Fig. 6 displays plots of the relevant data for our theoretical model from both Martini and Cooke simulations. The upper plots show the reduced area per lipid of the two leaflets (the independent variable $a = A/N_0$ in Eq. 17) as a function of asymmetry δn. The plotted blue curves are fits to the equilibrium area predicted by our theory, with optimal parameters found to be $\gamma = 0.54\,k_B T/\mathrm{nm}$, $\sigma = 0.747\,k_B T/\mathrm{nm}^2$, and $b = 0.729$ for Martini, and $\gamma = 3.5 \times 10^{-3} k_B T/\sigma^*$ $\sigma = 0.50\,k_B T/\sigma^{*2}$ for Cooke. One complication arising in the fitting process for the Cooke model was the influence of an extremely low line tension γ on the fitting of the barrier height parameter b. A value of $\gamma \ll k_B T/\sigma^*$ results in the finite-size free energy being nearly identical to the thermodynamic limit case, in which the nonconvex part of the free energy is replaced with the double-tangent line. In

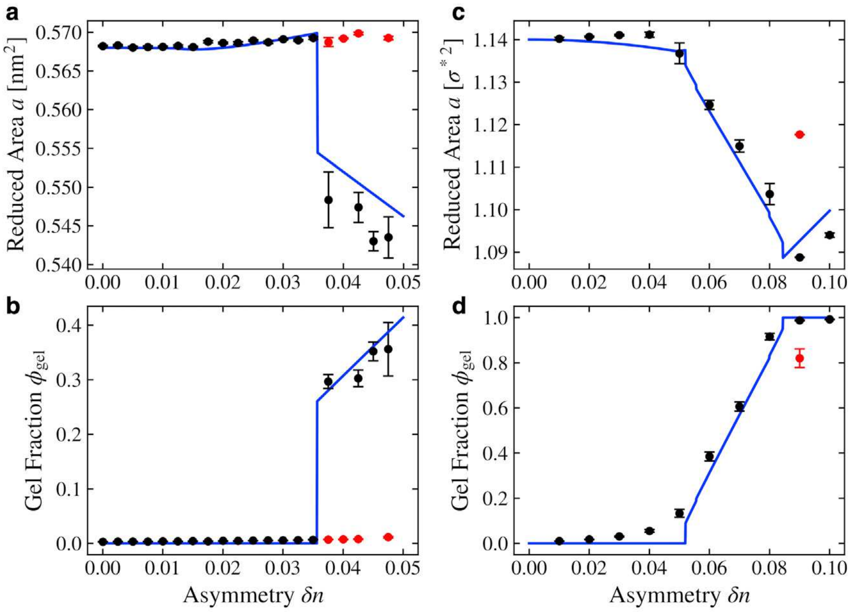

FIGURE 6 (*a*) Area of Martini DLPC membrane (*black circles*) at 297.5 K as a function of asymmetry along with curve of best fit (*blue*) to finite-size membrane theory. (*b*) Fraction of compressed leaflet identified to be in gel phase (*black circles*) as a function of asymmetry along with prediction by finite size theory (*blue*) using parameters from the fit in the top figure. (*c*) and (*d*) are the equivalent plots for the asymmetric Cooke model at $k_{\mathrm{B}}T = 1.36\varepsilon$. Red points indicate metastable states also visited during the simulation trajectories. For all simulation results, the area measurements are of the projected area of the membrane (the area of the principle simulation box). Error bars show the error of the mean. To see this figure in color, go online.

this region of parameter space, the value of b has essentially no impact on the predicted area and gel fraction, as the barrier is flattened to a line regardless of its height. As a result, b values obtained in fitting are essentially meaningless, with very large uncertainties. For this reason, fits for the Cooke model were performed with $b = 1$, the value for which the homogeneous free energy is smoothest. The value of b is meaningful for the Martini systems, however, as the sizable line tension leads to the realization of homogeneous barrier states not observed in the thermodynamic limit, resulting in obvious changes in the behavior of the system's area and phase composition as δn is varied.

Looking at the results qualitatively, for Martini the area increases slowly before sharply dropping between 3.5 and 3.75% asymmetry, and continuing downward thereafter. This sharp transition corresponds to the compressed leaflet transitioning from a uniformly strained fluid to a fluid and gel band coexistence state (see the schematic in Fig. 3 *b*). This behavior is clearly seen in simulation snapshots, and quantitatively identified by local changes in hexatic order and area per lipid. The Martini system never exhibits stable circular gel domains in these simulations, and instead goes directly from uniform fluid to gel band. This is largely a consequence of the simulation geometry, combined with a sizable line tension between the fluid and gel phases because, by the time a circular domain of gel would be stable, the domain would be large enough to connect across the short periodic box direction and form a band.

The Cooke data do not show a pronounced discontinuous transition, but rather a nearly continuous transition from uniformly strained fluid to fluid-gel coexistence. This is due to a remarkably low line tension between the fluid and gel phases, resulting in essentially negligible finite-size corrections as mentioned before. Such a low line tension is likely attributable to the ultra CG nature of the Cooke model. In addition, the robustness of the Cooke model allowed us to simulate to high enough asymmetry values that the compressed leaflet becomes entirely gel phase, which occurs beyond $\delta n \approx 9\%$. One may also notice that the area of the membrane trends slightly upward for the first few δn values, which is not captured by the theoretical fit. This is potentially due to the omission of higher-order area elasticity terms from the free energy, which were previously shown to remedy the discrepancy between Hookean predictions and simulation measurements of membrane area (25).

The lower plots in Fig. 6 show the fraction of the compressed leaflet identified by HMM as being in the gel phase, along with the theoretical *prediction* for the gel fraction based on the optimal parameters from the fit in the top figure. It can be seen that the parameters obtained from the area fitting produce very good agreement between predicted and observed phase coexistence.

DISCUSSION AND CONCLUSION

When the possibility of number asymmetry is allowed for a tensionless single-component lipid membrane, novel regions can appear in the phase diagram at temperatures sufficiently close to the main phase transition exhibiting the stable coexistence of fluid and gel domains. This phenomenon can be explained using very generic thermodynamic arguments (20). In fact, it should occur in the vicinity of *any* first-order phase transition exhibiting some "parallel coupling" of its extensive variable, as we have illustrated with our van der Waals "warm-up." In the case of membranes we required a few straightforward assumptions about the free energy of lipid monolayers near their main phase transition, but the basic phenomenology is independent of those.

The theory as framed thus far provides a method of predicting the gel content of individual leaflets as a function of imposed bilayer asymmetry. However, perhaps more interesting is the reverse: inferring bilayer asymmetry from observation of fluid-gel coexistence in the compressed leaflet of a bilayer. Differential stress is a difficult quantity to measure directly, because it is unclear how one would set up a mechanical coupling to a single leaflet. The framework presented here offers an indirect way of probing this aspect of asymmetry, potentially providing a way of calibrating asymmetric vesicle preparation methods with regard to the number asymmetry of the resultant membranes. This could be through measurement of the gel fraction of a leaflet, and subsequent matching to asymmetry by mapping out phase diagrams like those in Fig. 5. Alternatively, via slowly cooling fluid membranes one could observe the temperature of the onset of coexistence, which can be mapped to asymmetry by the simple approximation of Eq. 20, or to differential stress via Eq. 21. The practical feasibility of specific measurement strategies is another subject in its own right, but there at least now exists a connection between asymmetry and more readily observable quantities.

The phenomenon of the main phase transition in lipid bilayers being broadened from its sharp first-order nature is not in itself new (20,22,43). Markin and Kozlov proposed a theoretical explanation for the case where the transitions in the two leaflets are, for whatever reason, detuned from one another and the constraint due to elastic coupling forces a compromise. As a result, the main transition appears to be "smeared" over a temperature range that could be quite large if the two leaflets differ markedly in their T_{gel} (20). The analysis developed in (20) differs somewhat from ours, and does not investigate an elastic mismatch due to unequal lipid packing as a source of the detuning. All the same, it is important to bear in mind that fluid-gel coexistence in monolayers can be influenced by many factors, such as ion concentration in solution, as explored in their work.

The presence of gel domains significantly increases the effective bending modulus of the bilayer when measured in buckling simulations, and this phenomenon will likely have implications for experimental systems (16). Care must be taken, however, when trying to extrapolate these results to larger experimental systems, such as GUVs. The precise behavior of the gel domains in the compressed leaflet will determine whether the membrane as a whole appears to have a larger "effective" bending modulus or whether it must be treated as an inhomogeneous composite material. Definitive predictions in this regime would require consideration of physical processes not included in our model, such as curvature-mediated interactions between domains—a topic of potential future work.

Our current focus has been on the behavior of the compressed leaflet of the bilayer, even though the same equations yield predictions for the stretched leaflet as well. However, unlike the compressed leaflet, potentially interesting new behavior will only occur in the stretched leaflet for temperatures below the main phase transition, where the compressed leaflet is entirely in the gel phase. Therefore, we are hesitant to read too much into predictions in this regime given that the present theory includes no notion of interleaflet coupling, and one may well expect a leaflet entirely in the gel phase to significantly affect the behavior of its opposing leaflet. These state points also present a challenge with regard to the equilibration of gel-phase membranes in a simulation, as well as being experimentally difficult to work with. In addition, the conditions of most interest to biology are those above the main transition, as the membranes of living organisms almost invariably exist primarily in the fluid phase (44).

At this point it bears mentioning that the present theory, while capturing key qualitative features of the underlying physics, ignores a number of effects that could impact a quantitative comparison with experiments. One notable element is the interplay between differential stress and a difference in spontaneous leaflet curvature. In practice, these two phenomena should go hand in hand, but in fact *offset* one another; otherwise it is hard to explain how one can routinely create micron-sized asymmetric vesicles in experiment without them immediately creating tubules due to typically large unbalanced bending torques (15). Furthermore, biological membranes are composed of mixtures of a variety of lipids with wide-ranging properties, generally with pronounced composition asymmetry between the two monolayers (4), so that this type of torque compensation is likely to play a role in biomembrane elasticity.

For the specific situation discussed here—the emergence of gel domains—this issue arises in a particularly transparent way, because the tighter lipid packing in gel phases not only increases their rigidity but almost certainly also changes their spontaneous leaflet curvature (likely making it more positive, since the tails condense more than the heads; but no hard data seem to exist about this). Hence, the appearance of gel domains in only one leaflet should affect the local membrane shape. This is beyond the purview of our present theory, but it could matter for the macroscopically observable states, for instance, because sufficiently large gel domains could repel each other via curvature-mediated interactions and thus remain finite. Beyond that, the contact between a gel and a fluid leaflet should also have rather basic thermodynamic implications due to nonelastic interleaflet interactions (which we ignore). For instance, we expect that the presence of a fluid leaflet lowers the transition temperature in the gel leaflet (it is slightly harder to order in the presence of a fluctuating partner), while the opposite happens for the fluid leaflet.

TABLE 1 Glossary

Symbol	Description
$(\,)_\pm$	subscript denoting quantity in compressed (+) or expanded (−) subsystem
$(\,)_\mathrm{m}$	subscript denoting monolayer quantity
$(\,)_\mathrm{fl/gel}$	subscript denoting quantity in fluid/gel phase
a	reduced area, defined analogously to v
a_ℓ	equilibrium area per lipid
b	barrier height in monolayer free energy ansatz
K_A	area compressibility modulus
k_A	reduced area modulus, K_A/a_ℓ
δn	number asymmetry parameter, defined in Eq. 1
N_0	average number of molecules per subsystem
T_lv	liquid-vapor phase transition temperature
T_gel	fluid-gel phase transition temperature
T_pc	temperature of onset of phase coexistence, Eq. 20
v	reduced volume, defined in Eq. 5
γ	fluid-gel line tension
ε	energy unit in CG Cooke model simulations
σ	pretension/temperature analog in monolayer free energy ansatz
σ^*	length unit in CG Cooke model simulations
$\Sigma_\pm$	monolayer tension of respective leaflet (±)
Σ	bilayer net tension, $\Sigma = \Sigma_+ + \Sigma_-$
$\Delta\Sigma$	differential stress, $\Delta\Sigma = \Sigma_> - \Sigma_<$

Incorporating these considerations into the present model will be the subject of future work.

While gel phases only play a small role in biology, coexisting domains of liquid ordered phases embedded in a liquid disordered matrix are a widely discussed framework for understanding lipid rafts. They have been extensively studied in experiment (45–50), theory (51–56), and simulation (57–61), including in the compositionally asymmetric case (62–66). In the present context, this $L_\mathrm{o}/L_\mathrm{d}$ transition is particularly intriguing because its much smaller latent heat (compared with the gel/fluid transition) renders the slope of the phase boundary, $(\mathrm{d}\Sigma/\mathrm{d}T)_\mathrm{pb}$, almost an order of magnitude smaller (this is confirmed by both the Clausius-Clapeyron equation as well as direct measurements (67,68)). Because of this, differential stress should move the transition temperature about an order of magnitude more strongly: the quite achievable (15) value $\Delta\Sigma = 4\ \mathrm{mN/m}$ should result in a huge shift of about 10°C. This is not only eminently measurable but highly biologically significant, considering that nature seems to place cell membranes between 10 and 35°C above the temperature of phase separation (69,70)—larger but not too much larger than the changes that can alternatively be driven by differential stress.

We have demonstrated, generically, the theoretical basis of asymmetry-dependent behavior of first-order phase transitions in bilayers. While our model is currently idealized, it allows for the inclusion of additional free energy terms coupling to other relevant membrane properties, providing an avenue for improving the theory. Given the recent explosion of interest in asymmetric membranes, in particular differentially stressed ones, we hope this work will help to draw attention to an otherwise well-obscured aspect of membrane mechanics, and inspire continued work striving to elucidate the role of membrane asymmetry in biology.

GLOSSARY

In Table 1 we provide a glossary of symbols and notations used throughout the text. It is not comprehensive, but attempts to clarify items with the most potential for confusion.

SUPPORTING MATERIAL

Supporting material can be found online at https://doi.org/10.1016/j.bpj.2022.07.021.

AUTHOR CONTRIBUTIONS

M.D. suggested the subject and acquired funding for it. S.L.F. carried out Cooke simulations, analyzed data, and developed numerical routines for generating coexistence diagrams. A.H. carried out Martini simulations and analyzed data. S.L.F. and M.D. developed the theoretical framework. S.LF. and M.D. wrote the manuscript with input from A.H.

ACKNOWLEDGMENTS

The authors thank Derek Hamersly for initial insights that led to this work. M.D. gratefully acknowledges support by the National Science Foundation under grant CHE 2102316. S.L.F. gratefully acknowledges support from the Pittsburgh chapter of the ARCS Foundation.

DECLARATION OF INTERESTS

The authors declare no competing interests.

REFERENCES

1. Lodish, H., A. Berk, ..., K. C. M. Martin. 2016. Molecular Cell Biology, Eighth edition. W.H. Freeman.
2. van Meer, G. 2011. Dynamic transbilayer lipid asymmetry. *Cold Spring Harb. Perspect. Biol.* 3:a004671.
3. Kobayashi, T., and A. K. Menon. 2018. Transbilayer lipid asymmetry. *Curr. Biol.* 28:R386–R391.
4. Lorent, J. H., K. R. Levental, ..., I. Levental. 2020. Plasma membranes are asymmetric in lipid unsaturation, packing and protein shape. *Nat. Chem. Biol.* 16:644–652.
5. Contreras, F.-X., L. Sánchez-Magraner, ..., F. M. Goñi. 2010. Transbilayer (flip-flop) lipid motion and lipid scrambling in membranes. *FEBS Lett.* 584:1779–1786.
6. Verkleij, A. J., R. F. Zwaal, ..., L. L. van Deenen. 1973. The asymmetric distribution of phospholipids in the human red cell membrane. A combined study using phospholipases and freeze-etch electron microscopy. *Biochim. Biophys. Acta.* 323:178–193.
7. Pautot, S., B. J. Frisken, and D. A. Weitz. 2003. Engineering asymmetric vesicles. *Proc. Natl. Acad. Sci. USA.* 100:10718–10721.
8. Hamada, T., Y. Miura, ..., M. Takagi. 2008. Construction of asymmetric cell-sized lipid vesicles from lipid-coated water-in-oil microdroplets. *J. Phys. Chem. B.* 112:14678–14681.

9. Hu, P. C., S. Li, and N. Malmstadt. 2011. Microfluidic fabrication of asymmetric giant lipid vesicles. *ACS Appl. Mater. Interfaces.* 3:1434–1440.
10. Matosevic, S., and B. M. Paegel. 2013. Layer-by-layer cell membrane assembly. *Nat. Chem.* 5:958–963.
11. Cheng, H.-T., and E. London. 2011. Preparation and properties of asymmetric large unilamellar vesicles: interleaflet coupling in asymmetric vesicles is dependent on temperature but not curvature. *Biophys. J.* 100:2671–2678.
12. Chiantia, S., P. Schwille, …, E. London. 2011. Asymmetric GUVs prepared by MβCD-mediated lipid exchange: an FCS study. *Biophys. J.* 100:L1–L3.
13. Doktorova, M., F. A. Heberle, …, D. Marquardt. 2018. Preparation of asymmetric phospholipid vesicles for use as cell membrane models. *Nat. Protoc.* 13:2086–2101.
14. Enoki, T. A., and G. W. Feigenson. 2019. Asymmetric bilayers by hemifusion: method and leaflet behaviors. *Biophys. J.* 117:1037–1050.
15. Hossein, A., and M. Deserno. 2020. Spontaneous curvature, differential stress, and bending modulus of asymmetric lipid membranes. *Biophys. J.* 118:624–642.
16. Hossein, A., and M. Deserno. 2021. Stiffening transition in asymmetric lipid bilayers: the role of highly ordered domains and the effect of temperature and size. *J. Chem. Phys.* 154:014704.
17. Lu, L., W. J. Doak, …, P. R. Chiarot. 2016. Membrane mechanical properties of synthetic asymmetric phospholipid vesicles. *Soft Matter.* 12:7521–7528.
18. Karamdad, K., R. V. Law, …, O. Ces. 2016. Studying the effects of asymmetry on the bending rigidity of lipid membranes formed by microfluidics. *Chem. Commun.* 52:5277–5280.
19. Elani, Y., S. Purushothaman, …, O. Ces. 2015. Measurements of the effect of membrane asymmetry on the mechanical properties of lipid bilayers. *Chem. Commun.* 51:6976–6979.
20. Markin, V., and M. Kozlov. 1983. Inter-and intramembrane interactions and phase transitions. *Gen. Physiol. Biophys.* 2:201–215.
21. Swendsen, R. 2020. An Introduction to Statistical Mechanics and Thermodynamics. Oxford University Press.
22. Nagle, J. F. 1980. Theory of the main lipid bilayer phase transition. *Annu. Rev. Phys. Chem.* 31:157–196.
23. Marsh, D. 1996. Lateral pressure in membranes. *Biochim. Biophys. Acta.* 1286:183–223.
24. Tröster, A., F. Schmitz, …, K. Binder. 2017. Equilibrium between a droplet and surrounding vapor: a discussion of finite size effects. *J. Phys. Chem. B.* 122:3407–3417.
25. Foley, S., and M. Deserno. 2020. Stabilizing leaflet asymmetry under differential stress in a highly coarse-grained lipid membrane model. *J. Chem. Theor. Comput.* 16:7195–7206.
26. Nagle, J. F., R. Zhang, …, R. M. Suter. 1996. X-ray structure determination of fully hydrated L_α phase dipalmitoylphosphatidylcholine bilayers. *Biophys. J.* 70:1419–1431.
27. Grabielle-Madelmont, C., and R. Perron. 1983. Calorimetric studies on phospholipid–water systems: I. DL-Dipalmitoylphosphatidylcholine (DPPC)–Water system. *J. Colloid Interface Sci.* 95:471–482.
28. Rawicz, W., K. C. Olbrich, …, E. Evans. 2000. Effect of chain length and unsaturation on elasticity of lipid bilayers. *Biophys. J.* 79:328–339.
29. Marrink, S. J., H. J. Risselada, …, A. H. De Vries. 2007. The MARTINI force field: coarse grained model for biomolecular simulations. *J. Phys. Chem. B.* 111:7812–7824.
30. Coppock, P. S., and J. T. Kindt. 2010. Determination of phase transition temperatures for atomistic models of lipids from temperature-dependent stripe domain growth kinetics. *J. Phys. Chem. B.* 114:11468–11473.
31. Sodt, A. J., M. L. Sandar, …, E. Lyman. 2014. The molecular structure of the liquid-ordered phase of lipid bilayers. *J. Am. Chem. Soc.* 136:725–732.
32. Sodt, A. J., R. W. Pastor, and E. Lyman. 2015. Hexagonal substructure and hydrogen bonding in liquid-ordered phases containing palmitoyl sphingomyelin. *Biophys. J.* 109:948–955.
33. Flyvbjerg, H., and H. G. Petersen. 1989. Error estimates on averages of correlated data. *J. Chem. Phys.* 91:461–466.
34. Abraham, M. J., T. Murtola, …, E. Lindahl. 2015. GROMACS: high performance molecular simulations through multi-level parallelism from laptops to supercomputers. *SoftwareX.* 1-2:19–25.
35. Berendsen, H. J. C., J. P. M. Postma, …, J. R. Haak. 1984. Molecular dynamics with coupling to an external bath. *J. Chem. Phys.* 81:3684–3690.
36. Cooke, I. R., K. Kremer, and M. Deserno. 2005. Tunable generic model for fluid bilayer membranes. *Phys. Rev. E Stat. Nonlin. Soft Matter Phys.* 72:011506.
37. Kolb, A., and B. Dünweg. 1999. Optimized constant pressure stochastic dynamics. *J. Chem. Phys.* 111:4453–4459.
38. Weik, F., R. Weeber, …, C. Holm. 2019. ESPResSo 4.0–an extensible software package for simulating soft matter systems. *Eur. Phys. J. Spec. Top.* 227:1789–1816.
39. hmmlearn. https://github.com/hmmlearn/hmmlearn. Accessed: 2022-03-08.
40. Baum, L. E., T. Petrie, …, N. Weiss. 1970. A maximization technique occurring in the statistical analysis of probabilistic functions of Markov chains. *Ann. Math. Stat.* 41:164–171.
41. Viterbi, A. 1967. Error bounds for convolutional codes and an asymptotically optimum decoding algorithm. *IEEE Trans. Inf. Theory.* 13:260–269.
42. Virtanen, P., R. Gommers; …, SciPy 10 Contributors. 2020. SciPy 1.0: fundamental algorithms for scientific Computing in Python. *Nat. Methods.* 17:261–272.
43. Van Dael, H., P. Ceuterickx, …, F. H. Van Cauwelaert. 1982. The thermotropic transition of large unilamellar (LUV) vesicles of dimyristoyl phosphatidylcholine by Raman spectroscopy. *Biochem. Biophys. Res. Commun.* 104:173–180.
44. Singer, S. J., and G. L. Nicolson. 1971. The structure and chemistry of mammalian cell membranes. *Am. J. Pathol.* 65:427–437.
45. Feigenson, G. W., and J. T. Buboltz. 2001. Ternary phase diagram of dipalmitoyl-PC/dilauroyl-PC/cholesterol: nanoscopic domain formation driven by cholesterol. *Biophys. J.* 80:2775–2788.
46. Veatch, S. L., and S. L. Keller. 2002. Organization in lipid membranes containing cholesterol. *Phys. Rev. Lett.* 89:268101.
47. Veatch, S. L., and S. L. Keller. 2003. Separation of liquid phases in giant vesicles of ternary mixtures of phospholipids and cholesterol. *Biophys. J.* 85:3074–3083.
48. Veatch, S. L., and S. L. Keller. 2005. Seeing spots: complex phase behavior in simple membranes. *Biochim. Biophys. Acta.* 1746:172–185.
49. Baumgart, T., G. Hunt, …, G. W. Feigenson. 2007. Fluorescence probe partitioning between Lo/Ld phases in lipid membranes. *Biochim. Biophys. Acta.* 1768:2182–2194.
50. Heberle, F. A., and G. W. Feigenson. 2011. Phase separation in lipid membranes. *Cold Spring Harb. Perspect. Biol.* 3:a004630.
51. Huang, J., and G. W. Feigenson. 1999. A microscopic interaction model of maximum solubility of cholesterol in lipid bilayers. *Biophys. J.* 76:2142–2157.
52. Radhakrishnan, A., and H. McConnell. 2005. Condensed complexes in vesicles containing cholesterol and phospholipids. *Proc. Natl. Acad. Sci. USA.* 102:12662–12666.
53. Putzel, G. G., and M. Schick. 2008. Phenomenological model and phase behavior of saturated and unsaturated lipids and cholesterol. *Biophys. J.* 95:4756–4762.
54. Machta, B. B., S. Papanikolaou, …, S. L. Veatch. 2011. Minimal model of plasma membrane heterogeneity requires coupling cortical actin to criticality. *Biophys. J.* 100:1668–1677.

55. Shlomovitz, R., and M. Schick. 2013. Model of a raft in both leaves of an asymmetric lipid bilayer. *Biophys. J.* 105:1406–1413.

56. Shlomovitz, R., L. Maibaum, and M. Schick. 2014. Macroscopic phase separation, modulated phases, and microemulsions: a unified picture of rafts. *Biophys. J.* 106:1979–1985.

57. Risselada, H. J., and S. J. Marrink. 2008. The molecular face of lipid rafts in model membranes. *Proc. Natl. Acad. Sci. USA.* 105:17367–17372.

58. Baoukina, S., E. Mendez-Villuendas, and D. P. Tieleman. 2012. Molecular view of phase coexistence in lipid monolayers. *J. Am. Chem. Soc.* 134:17543–17553.

59. Hakobyan, D., and A. Heuer. 2014. Key molecular requirements for raft formation in lipid/cholesterol membranes. *PLoS One.* 9:e87369.

60. Carpenter, T. S., C. A. López, …, S. Gnanakaran. 2018. Capturing phase behavior of ternary lipid mixtures with a refined martini coarse-grained force field. *J. Chem. Theor. Comput.* 14:6050–6062.

61. Javanainen, M., B. Fabian, and H. Martinez-Seara. 2020. Comment on “Capturing phase behavior of ternary lipid mixtures with a refined martini coarse-grained force field”. Preprint at arXiv. https://doi.org/10.48550/arXiv.2009.07767.

62. Collins, M. D., and S. L. Keller. 2008. Tuning lipid mixtures to induce or suppress domain formation across leaflets of unsupported asymmetric bilayers. *Proc. Natl. Acad. Sci. USA.* 105:124–128.

63. May, S. 2009. Trans-monolayer coupling of fluid domains in lipid bilayers. *Soft Matter.* 5:3148–3156.

64. Galimzyanov, T. R., R. J. Molotkovsky, …, S. A. Akimov. 2015. Elastic membrane deformations govern interleaflet coupling of lipid-ordered domains. *Phys. Rev. Lett.* 115:088101.

65. Williamson, J. J., and P. D. Olmsted. 2015. Registered and antiregistered phase separation of mixed amphiphilic bilayers. *Biophys. J.* 108:1963–1976.

66. Fowler, P. W., J. J. Williamson, …, P. D. Olmsted. 2016. Roles of interleaflet coupling and hydrophobic mismatch in lipid membrane phase-separation kinetics. *J. Am. Chem. Soc.* 138:11633–11642.

67. Chen, D., and M. M. Santore. 2014. Large effect of membrane tension on the fluid–solid phase transitions of two-component phosphatidylcholine vesicles. *Proc. Natl. Acad. Sci. USA.* 111:179–184.

68. Portet, T., S. E. Gordon, and S. L. Keller. 2012. Increasing membrane tension decreases miscibility temperatures; an experimental demonstration via micropipette aspiration. *Biophys. J.* 103:L35–L37.

69. Levental, I., and S. Veatch. 2016. The continuing mystery of lipid rafts. *J. Mol. Biol.* 428:4749–4764.

70. Burns, M., K. Wisser, …, S. L. Veatch. 2017. Miscibility transition temperature scales with growth temperature in a zebrafish cell line. *Biophys. J.* 113:1212–1222.